10554 *Macromolecules* **2010**, *43*, 10554–10559
DOI: 10.1021/ma102075c

Macromolecules
ARTICLE

Effect of Mesophase Separation on the Crystallization Behavior of Olefin Block Copolymers

Jing Jin, Jiang Du,* Qinghua Xia, Yongri Liang, and Charles C. Han*

State Key Laboratory of Polymer Physics and Chemistry, Joint Laboratory of Polymer Science and Materials, Institute of Chemistry, Chinese Academy of Sciences, Beijing 100190, China

Received September 8, 2010; Revised Manuscript Received October 24, 2010

ABSTRACT: This paper investigates the effect of mesophase separation on the crystallization behavior of olefin block copolymers (OBCs) with different octene contents, which were synthesized by chain shuttling technology. Crystallization always occurs simultaneously but competitively with mesophase separation in OBCs. Because of the reason that the crystallization temperature is lower than the mesophase separation temperature for the OBCs, the mesophase separation can start first; large portions of the crystallizable hard blocks are confined in the mesophase-separated domains and could not contribute to the formation of radial lamellar stacks. In addition, the mesophase separation creates a stereo-hindrance effect; crystal lamellae could only grow through the interstitial space between the dispersed domains. As a result, large and compact crystals could not be formed. As the octene content increased in the sample, mesophase separation becomes more and more dominant, and the crystal morphology degrades sharply from spherulites to fragmentary lamella structures. It is found that increasing the annealing time during development of the mesophase-separated structure has a similar effect to increasing the octene content in the sample. However, all of the OBCs can form nearly the same crystalline morphology if the mesophase separation is suppressed, from which we can postulate that the nature of crystallization due to the crystallizable hard blocks in OBCs should be similar.

Introduction

Olefin block copolymers (OBCs) with new molecular architecture have recently been produced via a process called chain shuttling polymerization by The Dow Chemical Company.[1] These blocky copolymers consist of crystallizable ethylene−octene blocks with low octene content and high melting temperature (called hard blocks), alternating with amorphous ethylene−octene blocks with high octene content and low glass transition temperature (called soft blocks). The blocky copolymers differ from anionically polymerized and hydrogenated olefin block copolymers in having a statistical multiblock architecture with a distribution in block lengths and a distribution in the number of blocks per chain.[2] Compared to statistical ethylene−octene copolymers, the blocky architecture imparts substantially higher crystallization and melting temperatures while maintaining a low glass transition temperature.[3] Consequently, OBCs exhibit a superior balance of flexibility and heat resistance as well as significantly improved compression set and elastic recovery that give rise to many potential applications.[4−6]

Block copolymers are distinct for their unique microphase separation behavior.[7,8] Many of the attractive features of block copolymers are derived from their ability to form complex nanoscale morphologies that give interesting properties and enable a wide range of applications.[9−12] In semicrystalline block copolymer systems, microphase separation and crystallization always coexist; their phase morphology is dictated by the competition of these two coexisting processes, which are normally path dependent.[13−16] Because of the unique block structure, OBCs do not follow the traditional rules established for random block copolymers and polymer blends.[3,17,18] The block length polydispersity of OBCs has a profound impact on phase behavior, making the domain spacings much larger than expected for traditional block copolymers of similar molecular weight.[19] On the other hand, although subjected to the constraints imposed by covalently linked crystallizable and noncrystallizable blocks, the OBCs can form space-filling spherulites even when the crystallinity is as low as 7%,[3,17] in contrast to the small fringed micellar crystals of statistical copolymers. An understanding of the relationship between the unique mesophase separation and crystallization behaviors in OBCs is an important challenge, which greatly affects the morphology and properties of the materials. To our knowledge, this complexity remains unexplored.

In this paper, we describe the interplay between mesophase separation and crystallization in OBCs. Comparisons are made in four OBC samples with different octene contents. The crystallization behavior is studied by atomic force microscopy (AFM) and optical microscopy (OM), accompanied by thermal analysis. It is found that mesophase separation competes and restrains the crystallization process by consuming the crystallizable materials and creating the stereo-hindrance effect in the sample.

Experimental Section

The blocky ethylene−octene copolymers (OBCs) synthesized by the chain-shuttling method were supplied as pellets by The Dow Chemical Company together with information on molecular weight, octene content, and hard block content as given in Table 1.

Specimens weighing 5−10 mg were cut from pellets for thermal analysis. Thermograms were obtained on a Perkin-Elmer Series 7 differential scanning calorimeter (DSC). Scans were taken between 30 and 280 °C with a heating/cooling rate of 10 °C/min. A quenching experiment was performed from 280 to −100 °C at 300 °C/min to avoid the mesophase separation effect; then the

*Corresponding authors. E-mail: c.c.han@iccas.ac.cn (C.C.H.), dujiang@iccas.ac.cn (J.D.).

 Published on Web 11/19/2010

Table 1. Characteristics of Blocky Ethylene−Octene Copolymers[a]

sample	M_w (g/mol)	M_n (g/mol)	net octene content (mol %)	soft block octene content (mol %)	hard block octene content (mol %)	octene content difference Δ (mol %)	hard block content (wt %)
OBC S1	180 000	76 000	17.87	22.6	1.13	21.47	16
OBC S2	183 000	81 000	18.65	24.2	1.23	22.97	17
OBC S3	224 000	78 000	22.66	29.7	1.6	28.1	15
OBC S4	249 000	74 000	25.36	35.7	2.06	33.64	18

[a] Data were provided by The Dow Chemical Company.

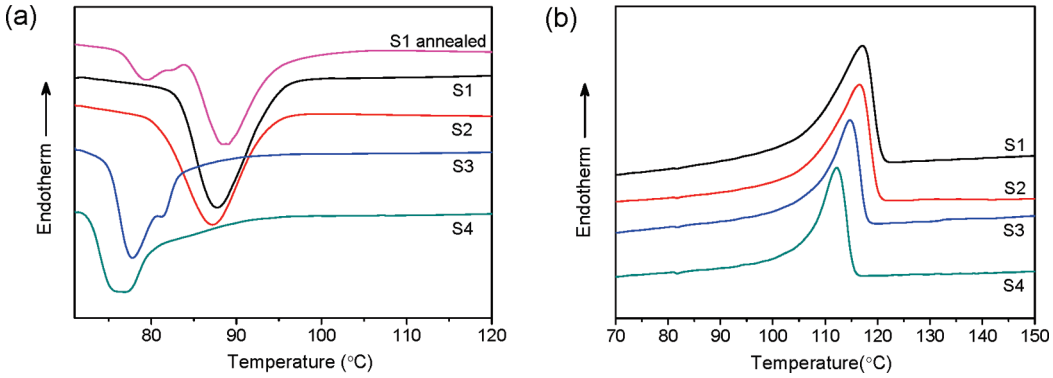

Figure 1. Thermal behavior of OBCs: (a) the crystallization process; (b) the melting process. The scan rate was 10 °C/min.

specimens were reheated to 200 °C at 10 °C/min. All the measurements were under a nitrogen atmosphere with a flow rate of 20 mL/min.

Specimens for atomic force microscopy (AFM) imaging were prepared from a 1% xylene solution dried on a silicon wafer. After heat treatment in Linkam-350 hot stage, free surfaces were imaged in air with a commercial scanning probe microscope Nanoscope III from Digital Instruments operating in the tapping mode. Images were collected at ambient conditions.

Specimens for optical microscopy (OM) were made by sandwiching a piece of pellet between two glass slides, heating at 200 °C for 5 min under a small pressure, and slowly cooling at ambient temperature. Polarized optical microscopy (POM) observation was performed on the specimens with an Olympus (BX51) microscope and an Olympus (C-5050) camera. A Linkam-350 hot stage was used to control the experimental temperature.

Results and Discussion

Figure 1 shows the DSC curves of crystallization (a) and the subsequent melting (b) of the four OBCs. The samples were first annealed at 280 °C for 5 min, then cooled to 30 °C at 10 °C/min, and reheated to 200 °C at the same rate. The values of crystallization temperature (T_c) and melting temperature (T_m), as well as heating transition enthalpies (ΔH_m) taken as the area of the melting peaks, are summarized in Table 2. Both the crystallization and melting temperatures are depressed from S1 to S4, as the octene content increased. The crystallinity of the OBCs also decreases from S1 to S4, as evidenced by the reduced enthalpy of melting. It is known that the DSC melting temperature is a statistical reflection of the thickness of lamella.[20] The lower melting temperature indicates thinner lamellae or lower degree of crystal perfectness in the sample when the octene content is increased. A second peak appears in the cooling curve of S3, and a broad peak appears in S4; however, there is only one sharp peak in S1 and S2. This indicates that fractional crystallization may occur in S3 and S4. Since there is little difference in the weight percentage and octene content of the crystallizable hard blocks in all of the OBCs, the observed changes should be mainly caused by the significantly increased octene content of the soft blocks in the samples. Interestingly, when S1 was annealed at 140 °C for 12 h before cooling to 30 °C, two evident crystallization peaks were also observed. We will discuss this point in later part of this section.

Table 2. Crystallization Temperature (T_c), Melting Temperature (T_m), and Melting Enthalpy (ΔH_m) of OBCs

sample	S1	S2	S3	S4
T_c (°C)	87.7	87.3	77.8	76.7
T_m (°C)	117.1	116.6	114.7	112.3
ΔH_m (J/g)	21.4	20.4	15.2	14.2

In order to explain the large differences in the thermal behavior of OBCs, the corresponding crystallization morphologies of S1 and S4 are observed by AFM after identical heat treatment as in the DSC measurements and are shown in Figure 2. S1 forms regular spherulites with typical radial lamellar structure, as shown in Figure 2a, similar to the crystalline structure of polyethylene homopolymer. However, in S4, there are obvious phase-separated spherical domains randomly dispersed in the matrix, as shown in Figure 2b. According to the component proportion, the dispersed phase should be the hard-block-rich phase, and the continuous phase should be the soft-block-rich phase. The average size of the dispersed domains is about 100 nm, which is much larger than the domain size of traditional microphase separation. Some papers have called this mesophase separation and suggested it is caused by polydispersity.[19] Crystal lamellae grow loosely among these mesophase-separated spheres and thus cannot form well-developed spherulites in S4. Crystallization and mesophase separation occur simultaneously, and hence competitively, in OBCs below the melting temperature. Figure 2a indicates that crystallization is the dominant process in S1, while Figure 2b indicates that mesophase separation proceeds dominantly (probably faster) in S4. As the octene content of the soft blocks increased from S1 to S4, the effect of mesophase separation becomes more important and the crystallization process is severely disturbed and confined. Since mesophase separation occurs intensively in S4, domains with different content of hard blocks are formed during cooling. When the temperature is further decreased, domains that are rich in hard blocks crystallize first and domains with fewer hard blocks crystallize afterward; in this way, fractional crystallization appears, which made a broad peak in the DSC cooling curve. When a mesophase separation process was imposed on S1 by holding the sample at 140 °C for

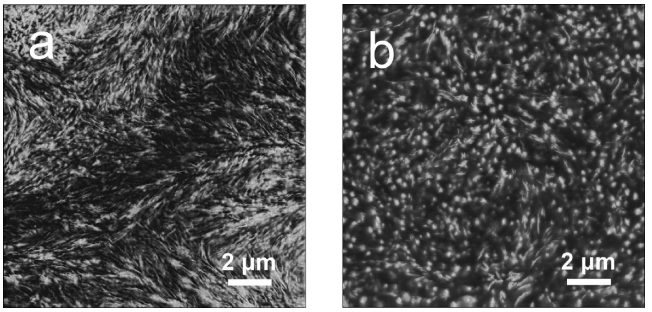

Figure 2. AFM images of nonisothermal crystallization morphology of S1 (a) and S4 (b) cooled from 280 to 30 °C at 10 °C/min; the same heat treatment as in the DSC measurements.

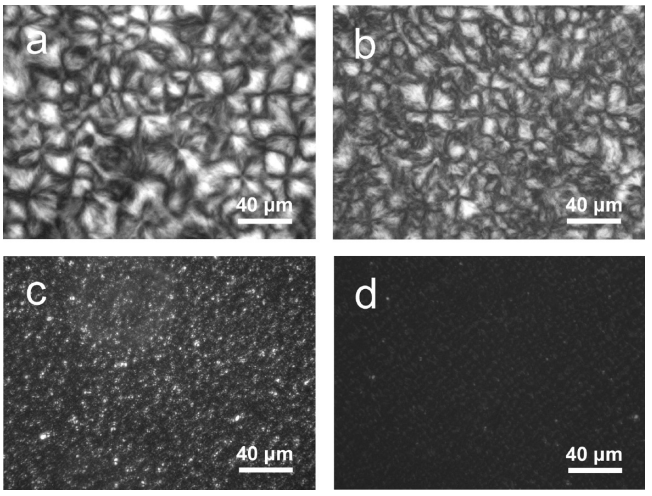

Figure 3. Polarized optical micrographs of OBCs crystallized at 110 °C for 12 h after annealing at 280 °C for 5 min: (a) S1, (b) S2, (c) S3, and (d) S4.

12 h (at this temperature, only mesophase separation proceeded while crystallization did not take place at all) before cooling to 30 °C at 10 °C/min, two crystallization peaks were also obtained, which confirms that fractional crystallization is caused by the mesophase separation effect.

Figure 3 shows the polarized optical micrographs of OBCs isothermally crystallized at 110 °C for 12 h after annealing at 280 °C for 5 min, illustrating the effect of increasing octene content on the crystallization behavior of OBCs. S1 forms well-developed, space-filling spherulites with the typical Maltese cross pattern and an average size of 20 μm in diameter, as shown in Figure 3a. S2 also forms spherulites. However, the average size of the spherulites in S2 is smaller than that in S1, and the distribution of spherulite size becomes broader in S2, as shown in Figure 3b. All the spherulites in S1 and S2 exhibit negative birefringence, which is typical for polyethylene spherulites. S3 only forms poorly developed spherulites. The dramatically reduced intensity of birefringence in S3 indicates that the crystallinity greatly decreases by increasing the octene content, as shown in Figure 3c. This trend becomes more evident as to S4, in which only small, nonspherulitic crystal fragments can be found (Figure 3d). Figure 3 indicates that the crystallization ability becomes weaker as the octene content increased from S1 to S4.

Figure 4 shows the in-situ DSC results of the OBCs' melting behavior after the samples being annealed at 280 °C for 5 min and then isothermally crystallized at 110 °C for 12 h. The melting peak and ΔH_m (J/g) are listed in Table 3. The crystallinity sharply decreases with increasing octene content from S1 to S4. There is almost no melting enthalpy that can be detected in S4 from the

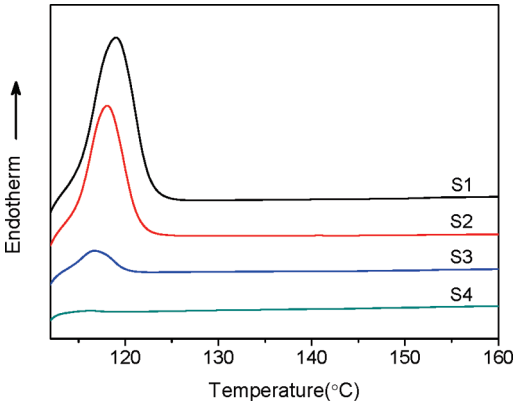

Figure 4. In-situ DSC results of reheating OBCs to 200 °C at 10 °C/min after annealing at 280 °C for 5 min and isothermal crystallization at 110 °C for 12 h.

Table 3. Melting Temperature and Melting Enthalpy of OBCs upon Reheating after Isothermal Crystallization

sample	S1	S2	S3	S4
T_m (°C)	119	118	117	–
ΔH_m (J/g)	20	13	2	–

measurement. Furthermore, the melting temperature also decreases with increasing octene content. Collectively, these data indicate that the crystallization behavior is remarkably different among these OBCs. This result is well matched with the morphologic observation by optical microscopy in Figure 3; the increasingly defective crystals and the dramatically reduced birefringence intensity from S1 to S4 reflect the sharply decreased crystallization ability.

AFM is a good method to provide further structural details of crystallization at substantially higher resolution than achievable by optical microscopy, especially in these semicrystalline block copolymers. Figure 5 shows the AFM results of the four OBC samples crystallized at 110 °C for 12 h after annealing at 280 °C for 5 min. These images clearly show the sharp changes of the crystal morphology from S1 to S4 with increasing octene content. S1 forms regular, compact, space-filling spherulites, as shown in Figure 5a. The lamellar stacks are relatively large and thick. The spherulites formed in S2 become irregular with more defects, as shown in Figure 5b. The lamellar stacks of S2 are not as compact as S1, and the mesophase-separated domains can be clearly observed in the interstices of the lamellar stacks. As for S3, the mesophase separation induces a "sea−island structure" as the primary morphology and the crystal lamellae are stacked loosely together that the sample is lack of well-developed spherulite structure, as shown in Figure 5c. It is obvious that lamella growth is restricted by the prior mesophase separation process and becomes discontinuous. In S4, crystallization is totally disturbed (Figure 5d), and the mesophase-separated morphology becomes dominant (Figure 5e). Fragmentary crystal lamellae could only grow along the interstitial regions between the previously formed mesophase-separated domains, as shown in Figure 5f.

From S1 to S4, the crystal morphology degrades sharply from spherulites to dispersed, small fragments of lamella structures. It should be noted that the AFM shows the surface images of the OBC solution-cast film, while the OM shows the bulk images of the OBC pellet hot-pressed between two glass slides. However, the morphological observation in Figure 5 is consistent with the result obtained by OM in Figure 3. They should reveal the same intrinsic nature of the sample. Well-organized lamella structures and demixed copolymer hard phase are also clearly seen by AFM in annealed pellets of S1 and S4 respectively (see Supporting Information Figure S1). It is clear that mesophase separation

occurs in the OBCs at 110 °C and even during the cooling process from 280 to 110 °C, which could severely impact on their crystallization behavior. The mesophase separation becomes more and more pronounced as the octene content increased from S1 to S4. Especially in S4, large portions of the crystallizable hard blocks assemble into spherical mesophase-separated domains before they could arrange into crystal lamellae when the sample is quenched to 110 °C; then the sample is hard to form lamella structures between these small discrete spherical domains. We suspect that the energy required to destroy the prior mesophase separation structure is too high to be overcome for the crystallization front under this condition. As a result, the previously formed spherical domains are undisturbed and, hence, the majority of crystalline material is confined to such domains. Consequently, large crystals could not be formed, and the overall crystallinity is severely hindered.

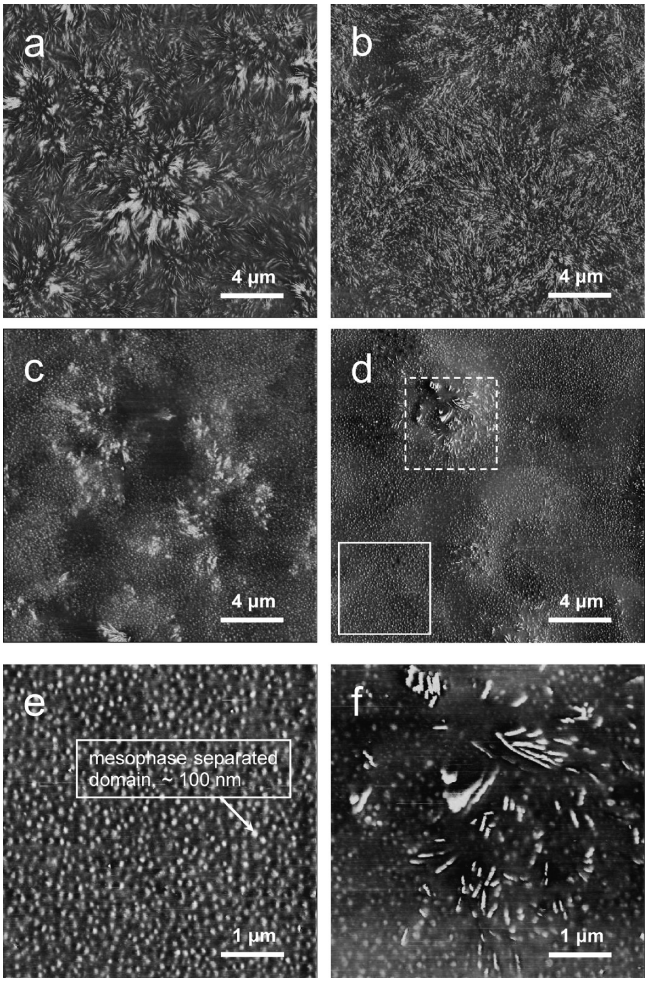

Figure 5. AFM images of OBCs crystallized at 110 °C for 12 h after annealing at 280 °C for 5 min: (a) S1, (b) S2, (c) S3, and (d) S4. (e) Magnified image of the solid box in (d). (f) Magnified image of the dashed box in (d).

Figure 6 shows the AFM images of S1 and S4 annealed at different temperatures for 5 min and then quenched into liquid nitrogen. A large number of random crystal lamellae and even undeveloped spherulites are formed during the quenching process in S1 when the initial annealing temperature is 240 °C, as shown in Figure 6a. However, mesophase separation morphology is dominant in S4 under the same condition, as shown in Figure 6b. The average size of the disperse domains is 80 nm, and the distance between these domains is about 100 nm, revealing fast kinetics of mesophase separation in S4. Interestingly, when the initial annealing temperature is increased to 280 °C, S4 also forms random crystal lamellae and undeveloped spherulites like S1, as shown in Figure 6c. The mesophase separation process in S4 is suppressed by annealing the sample at such a high temperature and quenching quickly into liquid nitrogen. This demonstrates that all of these OBC samples can form similar crystalline morphologies if mesophase separation is limited or suppressed.

Comparing Figure 6 with Figure 5, we conclude that although the nature of crystallization, due to the crystallizable hard blocks in the samples, is similar, the mesophase separation can greatly influence their crystallization behavior. As the difference in octene content between the soft and hard blocks becomes larger from S1 to S4, especially from S2 to S3, mesophase separation occurs much faster in S3 and S4 than in the other two samples. As a result, crystallization is restrained more severely in S3 and S4.

In Figure 7, we attempt to eliminate the mesophase separation process in the OBCs by quenching the samples very quickly from

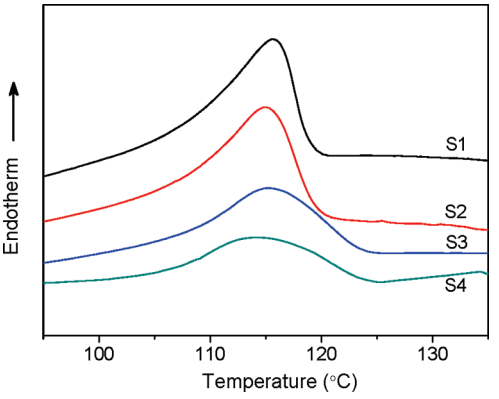

Figure 7. DSC traces of OBCs reheated to 200 °C at 10 °C/min after quenching from 280 to −100 °C at 300 °C/min.

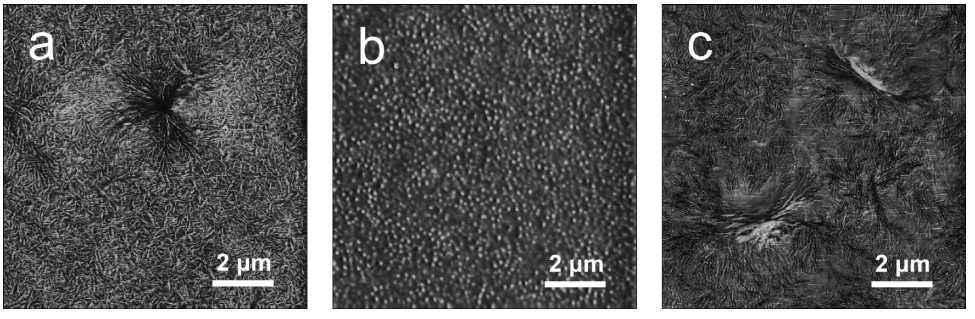

Figure 6. (a) AFM phase image of S1 annealed at 240 °C for 5 min, followed by rapidly quenching into liquid nitrogen. (b) AFM phase image of S4 annealed at 240 °C for 5 min, followed by rapidly quenching into liquid nitrogen. (c) AFM phase image of S4 annealed at 280 °C for 5 min, followed by rapidly quenching into liquid nitrogen.

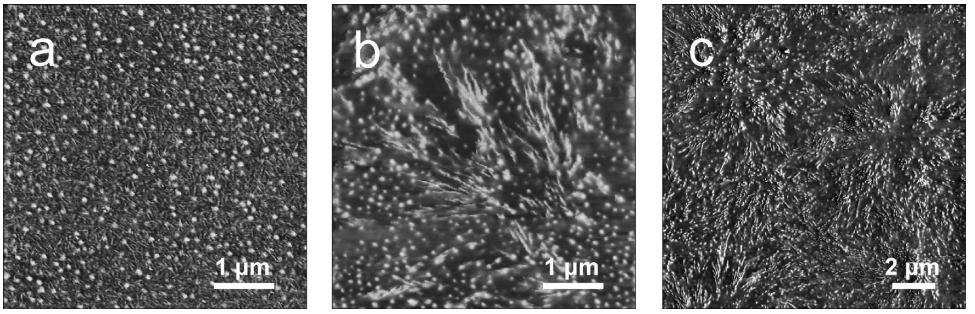

Figure 8. AFM images of S1 isothermally crystallized at 110 °C for (a) 0, (b) 2, and (c) 12 h after mesophase separation at 130 °C for 12 h, followed by rapidly quenching into liquid nitrogen.

high temperature; then the samples were reheated to 200 °C at 10 °C/min. The melting peak temperatures of the four OBC samples are almost the same this time, as shown in Figure 7. This result is quite different from Figure 1 but compatible with Figure 6 which shows all OBCs exhibit very similar crystalline structure when the mesophase separation effect is suppressed. It is known that there is almost no difference in the weight percentage of hard blocks in these OBCs. The decrease of melting enthalpy from S1 to S4 may partly originate from the increased octene content within the hard blocks.

In Figure 5, S1 can form large and perfect spherulites at 110 °C, while S4 cannot form spherulites under the same condition because of the effect of mesophase separation. If we impose a mesophase separation process on S1 before its crystallization at 110 °C, the spherulite structures should also be disturbed. In order to prove our deduction, the following experiment was carried out. S1 was first heated to 280 °C for 5 min, then quenched to 130 °C, and annealed for 12 h. In this process, mesophase separation proceeded markedly although slowly, while crystallization did not take place at all. As a result, a large number of spherical domains were formed and dispersed randomly in the matrix, as shown in Figure 8a. The average size of these domains is about 80 nm, and the distance between these domains is about 100 nm. If the sample was then quenched to 110 °C for crystallization, it was found that the previously formed spherical mesophase-separated domains maintained the dispersed state as in the melt when crystallization occurred. The crystal lamellae could only grow through the interstitial space between these domains, as shown in Figure 8b. Besides the stereo-hindrance effect of the mesophase separation, large portions of the crystallizable hard blocks were bound to be confined in the discrete domains and could not contribute to the formation of radial lamellar stacks. As a result, large and compact spherulites were not formed even after long crystallization time, as shown in Figure 8c. The loose crystals with discontinuous lamellar stacks are quite distinct from the well-developed crystalline morphology of S1 that directly crystallized at 110 °C without mesophase separation at 130 °C (Figure 5a). The effect of mesophase separation on the crystallization process is evident in this comparison.

We believe that the interference of mesophase separation in the crystallization will be even more pronounced at a higher crystallization temperature which will advance the mesophase separation process and suppress the crystallization process at the same time. Figure 9 shows the polarized optical micrographs of S1 crystallized at 120 °C (the previous crystallization temperature is fixed at 110 °C). Only very small crystals are formed after 1 day at 120 °C (Figure 9a). A Maltese cross can be faintly distinguished after 2 days (Figure 9b). It appears that the spherulites grow very slowly and are limited to small size (about 15 μm in diameter) even after crystallization at 120 °C for 4 days, as shown in Figure 9d. In addition, the structure of these spherulites is far

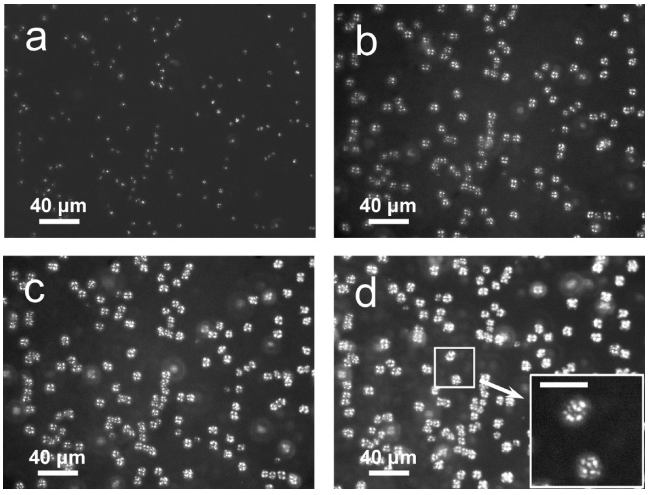

Figure 9. Polarized optical micrographs of S1 crystallized at 120 °C for (a) 1, (b) 2, (c) 3, and (d) 4 days after annealing at 280 °C for 5 min. The scale bar of the inset in (d) is 20 μm.

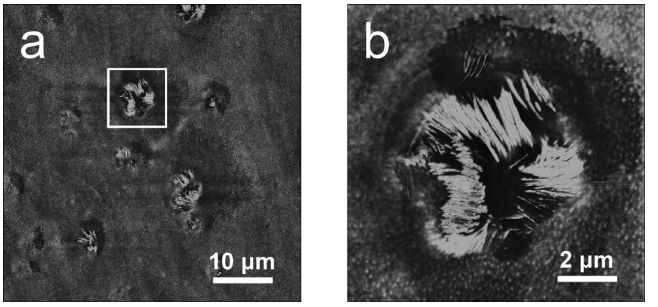

Figure 10. AFM images of S1 crystallized at 120 °C for 3 days after annealing at 280 °C for 5 min. (b) Magnified image of the solid box in (a).

from perfect. The inset of Figure 9d shows a kind of fragmentary Maltese cross pattern of the spherulites. Further structural details of such spherulites are obtained from AFM observation, as shown in Figure 10. The spherulite is more like a loose cluster of lamellar stacks rather than the typical spherulitic structure and appears to be surrounded and confined by a mass of mesophase-separated domains.

Conclusions

In this paper, we investigated the effect of mesophase separation on the crystallization behavior of olefin block copolymers with different octene contents, which were synthesized by chain shuttling technology. As the octene content increased from S1 to S4, mesophase separation becomes more and more dominant and

the crystal morphology degrades sharply from spherulites to dispersed small lamella structures. In this OBC system, crystallization and mesophase separation occur simultaneously in a competitive manner. If the mesophase separation is the dominant process, the formed spherical mesophase-separated domains maintain a dispersed state even after crystallization. Crystal lamellae could only grow through the interstitial space of these domains. Besides the stereo-hindrance effect, large portions of the crystallizable hard blocks are confined in the discrete mesophase-separated domains and could not contribute to the formation of radial lamellar stacks. As a result, large and compact crystals could not be formed. It is found that increasing the annealing time during development of the mesophase-separated structure has a similar effect as the increases in octene content. However, all of the OBCs form nearly the same crystalline morphology if the mesophase separation effect is suppressed, from which we could postulate that the nature of crystallization due to the crystallizable hard blocks should be similar.

Acknowledgment. This work was supported by National Natural Science Foundation of China (No. 50930003). The authors thank The Dow Chemical Company for kindly providing the samples.

Supporting Information Available: AFM image of the cross section of annealed OBC pellet. This material is available free of charge via the Internet at http://pubs.acs.org.

References and Notes

(1) Arriola, D. J.; Carnahan, E. M.; Hustad, P. D.; Kuhlman, R. L.; Wenzel, T. T. *Science* **2006**, *312*, 714–719.
(2) Shan, C. L. P.; Hazlitt, L. G. *Macromol. Symp.* **2007**, *257*, 80–93.
(3) Wang, H. P.; Khariwala, D. U.; Cheung, W.; Chum, S. P.; Hiltner, A.; Baer, E. *Macromolecules* **2007**, *40*, 2852–2862.
(4) Dias, P.; Lin, Y. J.; Poon, B.; Chen, H. Y.; Hiltner, A.; Baer, E. *Polymer* **2008**, *49*, 2937–2946.
(5) Lin, Y. J.; Yakovleva, V.; Chen, H. Y.; Hiltner, A.; Baer, E. *J. Appl. Polym. Sci.* **2009**, *113*, 1945–1952.
(6) Wang, H. P.; Chum, S. P.; Hiltner, A.; Baer, E. *J. Appl. Polym. Sci.* **2009**, *113*, 3236–3244.
(7) Bates, F. S.; Fredrickson, G. H. *Annu. Rev. Phys. Chem.* **1990**, *41*, 525–557.
(8) Bates, F. S.; Fredrickson, G. H. *Phys. Today* **1999**, *52*, 32–40.
(9) Mansky, P.; Chaikin, P. M.; Thomas, E. L. *J. Mater. Sci.* **1995**, *30*, 1987.
(10) Park, M.; Harrison, C.; Chaikin, P. M.; Register, R. A.; Adamson, D. H. *Science* **1997**, *276*, 1401.
(11) Huang, E.; Rockford, L.; Russell, T. P.; Hawker, C. J. *Nature* **1998**, *395*, 757.
(12) De Rosa, C.; Park, C.; Thomas, E. L.; Lotz, B. *Nature* **2000**, *405*, 433.
(13) Loo, Y. L.; Register, R. A.; Ryan, A. J. *Phys. Rev. Lett.* **2000**, *84*, 4120.
(14) Loo, Y. L.; Register, R. A.; Ryan, A. J. *Macromolecules* **2002**, *35*, 2365.
(15) Zhu, L.; Cheng, S. Z. D.; Calhoun, B. H.; Ge, Q.; Quirk, R. P.; Thomas, E. L.; Hsiao, B. S.; Yeh, F. *J. Am. Chem. Soc.* **2000**, *122*, 5957.
(16) Quiram, D. J.; Register, R. A.; Marchand, G. R.; Adamson, D. H. *Macromolecules* **1998**, *31*, 4891.
(17) Khariwala, D. U.; Taha, A.; Chum, S. P.; Hiltner, A.; Baer, E. *Polymer* **2008**, *49*, 1365–1375.
(18) Wang, H. P.; Chum, S. P.; Hiltner, A.; Baer, E. *J. Polym. Sci., Part B: Polym. Phys.* **2009**, *47*, 1313–1330.
(19) Hustad, P. D.; Marchand, G. R.; Garcia-Meitin, E. I.; Roberts, P. L.; Weinhold, J. D. *Macromolecules* **2009**, *42*, 3788–3794.
(20) Hoashi, K.; Mochizuki, T. *Makromol. Chem.* **1967**, *100*, 78–90.